⌘ *Author's Choice*

Disruption of the ATP-binding Cassette B7 (ABTM-1/ABCB7) Induces Oxidative Stress and Premature Cell Death in *Caenorhabditis elegans*[*][S]

Pilar González-Cabo[‡§], **Arantxa Bolinches-Amorós**[‡§], **Juan Cabello**[¶‖], **Sheila Ros**[‡], **Sergio Moreno**[¶], **Howard A. Baylis**[**], **Francesc Palau**[‡§], and **Rafael P. Vázquez-Manrique**[**][1]

From the [‡]Laboratory of Genetics and Molecular Medicine, Instituto de Biomedicina de Valencia, Consejo Superior de Investigaciones Científicas, 46010 Valencia, Spain, the [§]CIBER de Enfermedades Raras, 46010 Valencia, Spain, the [¶]Instituto de Biología Molecular y Celular del Cáncer, Centro de Investigación del Cáncer (Universidad de Salamanca-Consejo Superior de Investigaciones Científicas), Campus Universitario Miguel de Unamuno, 37007 Salamanca, Spain, the [‖]Oncology Area, Centre for Biomedical Research of La Rioja, 26006 Logrono, Spain, and the [**]Department of Zoology, University of Cambridge, Downing Street, Cambridge CB2 3EJ, United Kingdom

X-linked sideroblastic anemia with ataxia (XLSA/A) is a rare inherited disorder characterized by mild anemia and ataxia. XLSA/A is caused by mutations in the *ABCB7* gene, which encodes a member of the ATP-binding cassette transporter family. Studies in yeast, mammalian cells, and mice have shown that ABCB7 functions in the transport of iron-sulfur (Fe-S) clusters into the cytoplasm. To further investigate the mechanism of this disease, we have identified and characterized the *Caenorhabditis elegans* homologue of the *ABCB7* gene, *abtm-1*. We have studied the function of *abtm-1* using mutants and RNAi. *abtm-1*-depleted animals produce arrested embryos that have morphogenetic defects and unusual premature, putative apoptotic events. *abtm-1*(*RNAi*) animals also show accumulation of ferric iron and increased oxidative stress. Despite the increased level of oxidative stress in *abtm-1*(*RNAi*) animals, they have an increased life span. We observed accumulation of DAF-16/FOXO in the nuclei of affected animals and elevation of the expression of SOD-3, a well established target of DAF-16, which may explain the increased life span extension of these animals. *abtm-1* is strongly expressed in tissues with a high energy demand, and *abtm-1*(*RNAi*) animals have phenotypes that reflect the need for *abtm-1* in these tissues. Finally, we show that reducing the function of other genes involved in Fe-S cluster production produces similar phenotypic consequences to *abtm-1* loss of function. Therefore, ablation of *abtm-1* in *C. elegans* provides a model in which to investigate the mechanism underlying XLSA/A.

X-linked sideroblastic anemia with ataxia (XLSA/A[2]; OMIM 301310) is a rare inherited disorder in which male patients suffer from mild anemia together with a nonprogressive and early onset ataxia characterized by dysmetria and dysdiadochokinesis (1). Other reported symptoms include dysarthria, intention tremor, mild learning disability, and depression. XLSA/A-associated anemia is mild and asymptomatic in males. Female carriers usually do not show anemia or neurological conditions. XLSA/A is caused by mutations in *ABCB7*, a gene located at position Xql3 (2). *ABCB7* encodes a highly conserved protein belonging to the ABCB family of ATP-binding cassette (ABC) transporters (3). Members of the ABC superfamily are transmembrane proteins that use the hydrolysis of ATP to facilitate transport of a range of substrates across membranes.

Analyses of three different families with XLSA/A have identified three associated mutations in the *ABCB7* gene. Two of these are missense mutations, which cause the substitution of residues within the ABCB7 transmembrane domains: V411L (4) and I400M (2). The third mutation produces a more substantial amino acid change E433K (5). A human cDNA containing the E433K change is able to partially rescue yeast carrying a mutation in *ATM1*, the homologue of *ABCB7*, suggesting that this change does not cause a complete loss of function (5). Thus, no complete loss of function mutations in this gene have been described, suggesting that ABCB7 is an essential molecule. In support of this suggestion, *ABCB7* knock-out stem cells, hemizygous mice, and mice with conditional knock-outs in the central nervous system or bone marrow are all inviable (6, 7).

Studies in yeast have shown that Atm1p localizes to the mitochondrial inner membrane, and it has been suggested that this molecule is involved in the transport of iron-sulfur (Fe-S) clusters from the lumen of mitochondria to the cytosol (8, 9). Moreover, work performed with conditional knock-out ABCB7 mice suggests that mammalian ABCB7 transporters are also involved in Fe-S cluster assembly (6). Thus, mammalian (10) and yeast (8) *ABCB7/ATM1*-deficient cells show mitochondrial iron accumulation presumably because Fe-S clusters cannot be

⌘ *Author's Choice*—Final version full access.

[S] The on-line version of this article (available at http://www.jbc.org) contains supplemental "Experimental Procedures," "Results," Figs. S1–S3, and Tables S1–S3.

[1] To whom correspondence should be addressed: Laboratory of Neuronal Cell Biology and Pathology, Psychiatry and Neuroscience Center U894, INSERM, 2ter Rue d'Alesia 75014 Paris, France. Tel.: 33-1-40-78-86-63; Fax: 33-1-45-80-72-93; E-mail: rafael.vazquez@inserm.fr.

[2] The abbreviations used are: XLSA/A, X-linked sideroblastic anemia with ataxia; ABC, ATP-binding cassette; *cat*, chloramphenicol acetyltransferase; ML, median life span.

transferred to the cytosol. It is believed that this accumulation of mitochondrial iron causes oxidative stress, probably by the catalytic production of hydroxyl radicals, which then react with other biologically important molecules such as proteins, lipids, or DNA. This mitochondrial stress may then cause cellular dysfunction in the nervous system of patients. In addition, the impairment of iron homeostasis due to a lack of ABCB7 activity, directly or indirectly, disrupts the heme synthesis pathway, because Fe-S cluster assembly is essential for heme production (11), and it is this change that is responsible for the anemia of XLSA/A patients (7). Therefore, XLSA/A is a mitochondrial disease caused by a mutation of a nuclear gene involved in Fe-S cluster biosynthesis.

In this study, we used *Caenorhabditis elegans* to establish a model for the investigation of the molecular basis of XLSA/A. To do this, we have investigated the effect of depletion of *abtm-1/ABCB7* using mutant worms and by RNAi. We report that reduction of *abtm-1* function causes embryonic lethality during morphogenesis. We show that there is premature, putative apoptosis in *abtm-1(RNAi)* embryos that compromises the development of some cell lineages and may thus account for the increased embryonic lethality. *abtm-1(RNAi)* animals that reach adulthood show evidence of increased oxidative stress and accumulate ferric iron (Fe^{3+}), which may produce free radicals. We have also found that *abtm-1(RNAi)* worms have a pattern of alterations in life span, defecation, motility, and other behaviors indicative of mitochondrial impairment. We show increased expression of SOD-3 (superoxide dismutase), a well known DAF-16/FOXO target, and nuclear localization of DAF-16/FOXO in *abtm-1(RNAi)* animals. These adaptations to stress may partially account for the observed life span extension. Analysis of the expression pattern of *abtm-1* shows that the gene is strongly expressed in tissues that are likely to have a high demand for ATP. We also show that ablating other components of the Fe-S cluster synthesis pathway recapitulates some of the phenotypes observed in *abtm-1*-deficient animals.

EXPERIMENTAL PROCEDURES

Isolation of the abtm-1 cDNA—To identify the 5′ end of the cDNA, we used the sequence of the spliced leader, SL1, as a forward primer, and a gene-specific oligonucleotide as the reverse primer. The 3′ end was determined using rapid amplification of 3′-complementary DNA ends. Both products were cloned into pGEM-T (Promega, Madison, WI) and sequenced. We used primers designed using the information obtained from these clones to amplify the full-length cDNA. All products were cloned and sequenced to obtain the whole structure of *abtm-1*. The coding sequence of the gene does not differ significantly from the predicted spliced gene in the WormBase (release WS181) (NCBI accession number AF490975) (supplemental Fig. S1A).

Worm Culture and Strains—Worms were cultured using standard techniques and media (12). Strains used in this work are listed in supplemental Table S2. We out-crossed *abtm-1(tm2721)*, a gift from S. Mitani, four times before any phenotypic analysis was performed. After outcrossing, *abtm-1(tm2721)* males were crossed to KR344, which carries the free duplication *sDp2*. F2 hermaphrodites carrying *sDp2* and

tm2721 in homozygosis were isolated. All strains were maintained at 20 °C, unless otherwise stated.

Construction of Transgenic Worms—We used a PCR-based fusion approach to make *abtm-1::GFP* constructs. Both constructs also contain the 3′-UTR from *unc-54*. To produce the mitochondrial construct, *abtm-1::GFP1*, we fused a region containing the putative promoter and the first three exons of the *abtm-1* gene to GFP (Fig. 1A). The primers used were as follows: forward primer FP1175, 5′ CTC ACG ATT GAA ACG GAC CCG, and reverse primer FP784, 5′ AGT CGA CCT GCA GGC ATG CAA GCT TAC TTG ACT ACT GGC TCC CGG. The peptide produced by this construct contains the putative mitochondrial signal peptide. To obtain the cytoplasmic construct, *abtm-1::GFP2* (Fig. 1A), we amplified the region contained between the upstream gene, *eif-3*, and the first codon of *abtm-1* (forward primer FP1178, 5′ CCT ATT TTT GAA GGT TTC TGC G; reverse primer FP814, 5′ AGT CGA CCT GCA GGC ATG CAA GCT CAT TAT CGA TCT CTG AAA ACT GGA TTC GG). Both reverse primers used to make the constructs contain a sequence that overlaps the GFP sequence to allow fusion by PCR. To obtain transgenic animals, we injected 1–2 ng/μl of the test DNA together with 60 ng/μl of pRF4 as a marker, and 60 ng/μl of genomic DNA from wild type worms, digested with XhoI, as a DNA carrier, using methods described before (13).

Cellular Localization of ABTM-1—Hermaphrodites carrying extrachromosomal arrays containing *abtm-1::GFP1* were incubated at 25 °C for an hour in 50 μM MitoTracker® Red CMXRos (Invitrogen) and 1.8 mM 4′,6-diamidino-2-phenylindole (DAPI), diluted in M9 buffer (12). These animals were allowed to recover on fresh NGM plates for an hour at 20 °C. Then worms were anesthetized using 20 mM sodium azide in M9 buffer and mounted for microscopy on 2% agarose pads. Images were acquired using a Leica SP5 confocal microscope (Leica Microsystems GmbH, Wetzlar, Germany).

RNA Interference—RNAi was carried out by injection of dsRNA. dsRNA was synthesized *in vitro*, using template fragments between 400 and 700 bp, from the appropriate ORF, amplified by PCR using primers described in supplemental Table S3, and cloned into pGEM-T (Promega). dsRNA was made using T7 and SP6 RNA polymerases (Invitrogen) and combining the two single-stranded molecules, as described before (14). As a control, we used dsRNA from the *Escherichia coli* chloramphenicol acetyltransferase (*cat*) gene. Several young adult hermaphrodites were injected in the gonads (13). Injected worms were transferred after 18 h and phenotypes analyzed in the post-18-h offspring. Phenotypes were scored as described below.

Analysis of Embryonic Lethality and Larval Arrest—To investigate embryonic lethality in RNAi experiments, we collected embryos from animals after 24 and 38 h following the injection of dsRNA. Then we removed the parents and allowed the embryos to develop fully for 24 h before counting the number of arrested embryos and larvae. To investigate lethality from mutant strains, we did the same, but for the entire fertile period of the adults. We used 10–12 parental animals per strain per experiment. We considered embryos as arrested when they failed to hatch within 24 h. We considered larvae as arrested

when they did not progress to adulthood within 48 h of hatching.

To further analyze embryonic development, embryos were isolated by dissection and then mounted in embryo culture medium (15). To determine the terminal phenotype, embryos were left for 18 h at 20 °C. Confocal microscopy was performed using a Leica SP5 confocal microscope. Embryos for four-dimensional microscopy analysis were prepared as described (16). Eight *abtm-1*(RNAi) and three wild type embryos were mounted, at a very early stage (usually the two-cell stage), and recording of their development was carried out at 25 °C for 10 h at intervals of 60 s, with 25 different focal planes (1 μm separation), using a Zeiss Axioplan microscope (Carl Zeiss STM GmbH, Germany) equipped with Nomarski optics adapted as described (16). Cell lineage of the recorded embryos was subsequently traced using SIMI Biocell (SIMI GmbH, Germany).

Protein Extraction—Worms were collected from plates by washing with M9 buffer and transferred to screw cap tubes. The tubes were shaken gently for 20 min at room temperature to allow digestion of bacteria. Worms were collected by sedimentation and washed three times with M9 buffer. Five volumes of ice-cold lysis buffer (150 mM NaCl, 50 mM Tris-HCl, pH 8, 1% Nonidet P-40, and protease inhibitor mixture) were added to the worm pellets, and the mixture was homogenized using glass homogenizer during a 30-min period to allow cuticle breakdown. Lysates were centrifuged at 10,000 $\times$ *g* for 30 min, and the supernatant was collected for use in further analysis. Protein concentrations were determined by the Bradford method.

Iron Measurement—To determine the iron content of the worms, we used a BioVision iron assay kit (BioVision, Mountain View, CA). Protein samples from ~3000 *atm-1*(RNAi), or *cat*(RNAi), or *frh-1*(*ok610*), or N2 worms were tested for ferrous (Fe^{2+}), ferric (Fe^{3+}), and total (Fe^{2+} + Fe^{3+}) iron following the manufacturer's instructions.

Oxidative Stress Assays—To measure sensitivity to oxidative stress, 80 *abtm-1*(RNAi) or *cat*(RNAi) L4 larvae were incubated in the presence of 0, 0.5, 5, and 10 mM paraquat (methyl viologen, Sigma). The experiments were carried out for 3 days at 25 °C, as described previously (17). We scored worm survival each day, using the same protocol as for life span assays.

To analyze protein carbonylation we used an Oxyblot™ protein oxidation detection kit (Millipore, Billerica, MA). Briefly, worm lysate, prepared as above, containing 15 μg of protein was incubated in 12% SDS supplemented with 2,4-dinitrophenylhydrazine for 10 min at room temperature. Samples were resolved on a 12% SDS-PAGE, and 2,4-dinitrophenylhydrazine-derivatized proteins were detected by immunoblot using an anti-2,4-dinitrophenylhydrazine antibody.

In vivo analysis of *sod-3* and *daf-16* reporters-*sod-3* expression was analyzed using the KN259 (*huIs33*[*sod-3p::sod-3::GFP+pRF4(rol-6(su1006)*]) reporter strain. To quantify *sod-3*::GFP expression, we collected fluorescence images of more than 30 animals for each condition (*abtm-1*(RNAi) or *cat*(RNAi)). We then measured the pixels produced by fluorescence in the whole body of animals and determined the fluorescence level relative to worm area, using ImageJ. To investigate the cellular localization of DAF-16, we used the strain TJ365 (*zIs356*[*daf-16p::daf-16::GFP*; *rol-6(su1006)*]). We analyzed

control and *abtm-1*(RNAi) young adults produced by independently injected hermaphrodites (number of observed animals per strain $\geq$300). We observed the worms under a dissecting microscope, equipped with fluorescence. Animals were kept on plates with food, at 20 °C, and positives were scored when the animals presented fluorescent nuclei in one or more tissues. As a positive control we used animals under starving conditions.

Life Span Assays—To measure life span, L4 larvae were cultured at 20 °C on NGM with 0.1 g/ml of 5-fluorodeoxyuridine (Sigma) until death. Death was assessed by the response of the animal to gentle nose touch. Worm survival was counted every 24 h. Missing worms were scored as censored data. We scored more than 200 worms per sample.

Statistical Analyzes—All data are presented as means $\pm$ S.E. or as % of population. To assess statistical significance, we compared different populations using Student's two-tailed *t* test using GraphPad on line. To compare survival curves from life span and oxidative stress assays, we used the log-rank (Mantel-Cox) test, contained within the GraphPad Prism software (GraphPad Software, Inc., La Jolla, CA).

RESULTS

C. elegans ABCB7 Homologue, ABTM-1, Is a Mitochondrial Protein That Is Highly Expressed in Mitochondrion-rich Tissues—To identify homologues of ABCB7 in *C. elegans*, we used the human ABCB7 (hABCB7) sequence to search the *C. elegans* genome. We found that *abtm-1* (Y74C10AR.3) (Fig. 1*A*) shows high similarity to hABCB7. We cloned the *abtm-1* cDNA using RT-PCR. The *abtm-1* cDNA is 2504 bp long (supplemental Fig. S1*A*) and encodes a predicted protein of 703 residues. The C-terminal region of the predicted peptide, ABTM-1, is 51% identical to hABCB7 (supplemental Fig. S1*B*). ABTM-1 has the typical ABC superfamily structure, with six transmembrane domains and an ATP binding domain (supplemental Fig. S1*B*). Alignment of the protein sequence with sequences from the human and yeast ABCB7 family shows that ABTM-1 clusters within this family (supplemental Fig. S1*C*), strongly suggesting that this protein belongs to the ABCB7 transporter group. Analysis of ABTM-1 using the Mitoprot program (18) gave a probability of 99.4% that ABTM-1 is mitochondrial. To demonstrate that ABTM-1 is indeed a mitochondrial protein, we produced transgenic animals carrying an *abtm-1*::GFP fusion (*abtm-1*::*GFP1*, Fig. 1*A*) in which GFP is fused to the end of the third exon of *abtm-1.* The predicted peptide should contain the first 67 amino acids of the protein, including the predicted mitochondrial localization signal. We incubated transgenic worms carrying *abtm-1*::*GFP1* with a mitochondrial marker, MitoTracker® Red CMXRos (Molecular Probes). Confocal microscopy of these worms shows that ABTM-1::GFP1 clearly co-localizes with the mitochondrial marker (Fig. 1*B*) confirming that ABTM-1 is a mitochondrial protein and the *C. elegans* homologue of hABCB7.

We sought to investigate the expression pattern of *abmt-1* using the *abtm-1*::*GFP1* fusion; however, this construct resulted in some toxicity (data not shown). We therefore produced a cytoplasmic GFP construct, *abtm-1*::*GFP2*, in which the first codon of *abtm-1* was fused to GFP (Fig. 1*A*). Trans-
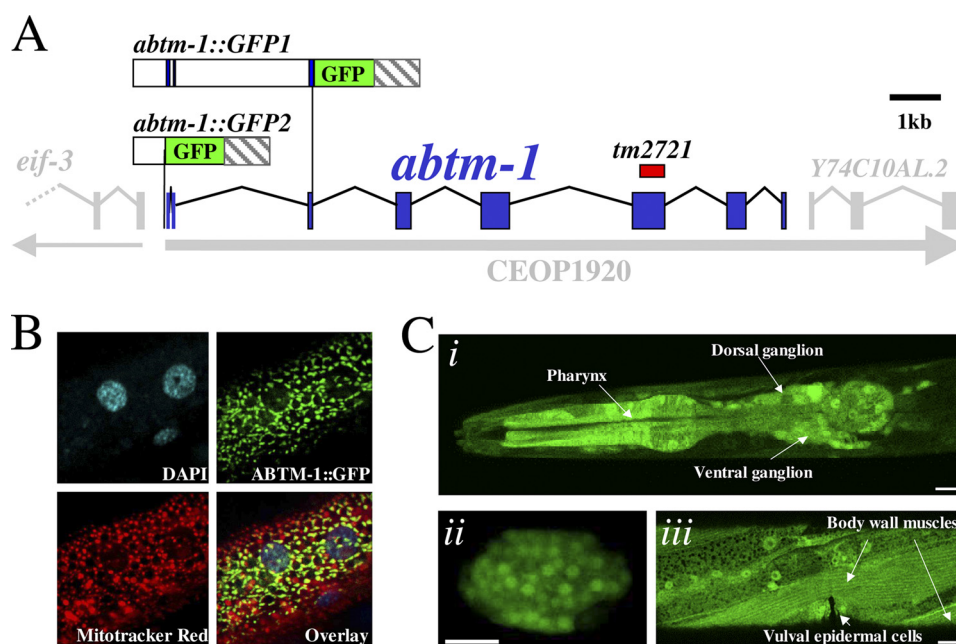
FIGURE 1. ***abtm-1* gene is the homologue of human *ABCB7*.** *A*, genomic structure of *abtm-1*. The *gray arrow below* the gene indicates that *abtm-1* is contained within an operon, OP1920, which contains another gene, *Y74C10AL.2*. The *red box above* the gene shows the position of the deletion in *abtm-1(tm2721)*. This diagram also shows the two GFP translational fusions used in this work. *Blue boxes* indicate exons of *abtm-1*. *B*, confocal microscope images showing co-localization of ABTM-1::GFP with Mitotracker Red, in muscle cells from adult hermaphrodites. *C*, *abtm-1*::GFP2 is highly expressed in the pharynx and neurons of the ventral and dorsal ganglions (*panel i*), developing embryos (*panel ii*), and body wall muscles and epidermis (*panel iii*).

genic animals containing *abtm-1*::GFP2 show widespread expression in the tissues of adult hermaphrodites, including the intestine, spermatheca, epidermis, and coelomocytes, among others (data not shown). Interestingly, *abtm-1*::GFP2 is highly expressed in tissues that are predicted to require high levels of energy production such as pharyngeal muscles (Fig. 1*C, panel i*), neurons (Fig. 1*C, panel i*), developing embryos (Fig. 1*C, panel ii*), and body wall muscles (Fig. 1*C, panel iii*), among others.

Worms Carrying a Deletion in abtm-1 Are Not Viable—We obtained a strain carrying a deletion and, probably null allele of *abtm-1, abtm-1(tm2721)* (Fig. 1*A*). The *tm2721* allele was outcrossed and balanced with *sDp2*, a duplication of the region of chromosome I carrying the *abtm-1* gene thus, allowing us to maintain *tm2721*. *sDp2* is a free duplication that undergoes random, non-Mendelian segregation with either copy of chromosome I during meiosis (19). Hermaphrodites carrying mutations that map in the region balanced with *sDp2* segregate, about 38% unbalanced mutant homozygotes (19). We isolated and analyzed three *abtm-1(tm2721)*I; *sDp2(I;f)* strains from independent crosses. We were unable to isolate viable homozygous unbalanced animals from these strains. We observed that the balanced animals produced $28.1 \pm 1.1\%$ arrested embryos and $7.1 \pm 0.6\%$ arrested L1-L2 larvae (wild type $1.2 \pm 0.2\%$ and 0% arrested embryos and larvae). The total lethality is therefore 35.2%, which is close to the predicted value of 38% for homozygous animals. This experiment strongly suggests that *abmt-1(tm2721)* homozygous animals exhibit early lethality and are unable to develop to adulthood.

RNAi of abtm-1 Induces Embryonic Arrest during Late Embryogenesis—Because complete ablation of *abtm-1* is lethal, we sought to emulate the condition of XLSA/A patients by reducing, rather than completely removing, the function of the

abtm-1 gene. To do this we used RNAi (*abtm-1(RNAi)*). We injected double-stranded *abtm-1* RNA into young wild type hermaphrodites to induce RNAi and then examined the resulting offspring. In agreement with results obtained using *abmt-1(tm2721)* embryos, we observed that reducing ABTM-1 in wild type hermaphrodites induces embryonic arrest in their offspring, $28 \pm 1.24\%$ (Fig. 2*A*). This lethality is further increased to $56 \pm 2.7\%$ in *daf-16*/FOXO mutants (Fig. 2*A*). DAF-16 is widely involved in insulin signaling and stress responses in *C. elegans* (20). Thus *daf-16* can protect against *abtm-1(RNAi)*-induced lethality, suggesting that the lethality may result from increased stress of some kind.

To further analyze the nature of the defects in *abtm-1(RNAi)*, we observed them under a differential interference contrast microscope. Some *abtm-1(RNAi)* embryos, 7.7%, arrested during the early proliferative stages (Fig. 2*B*); however, most of the arrested embryos showed clear signs of cell differentiation (Fig. 2*C*). For example, *abtm-1(RNAi)* embryos had gut granules indicating that the intestinal cells had differentiated (Fig. 2*C, panel ii*) and also showed vigorous twitching, an indicator of muscle cell differentiation. As the embryos arrested after gastrulation, we analyzed the behavior of epidermis, which plays a major role during embryonic morphogenesis (21, 22). To do this we used an epithelial cell-specific marker, *ajm-1*::GFP (22). 92.3% of arrested *abtm-1(RNAi)* embryos showed correctly (*i.e.* apically) localized AJM-1::GFP ($n = 104$) (Fig. 2*C, panels ii–iv*), suggesting that the epidermal cells are also differentiated. Nevertheless, analysis of the pattern of AJM-1::GFP revealed that most embryos show a highly disorganized structure, including a retracted epidermis (Fig. 2*C, panels ii* and *iii*), and the presence of internal tissues on the exterior of the embryo (Fig. 2*C, panel*
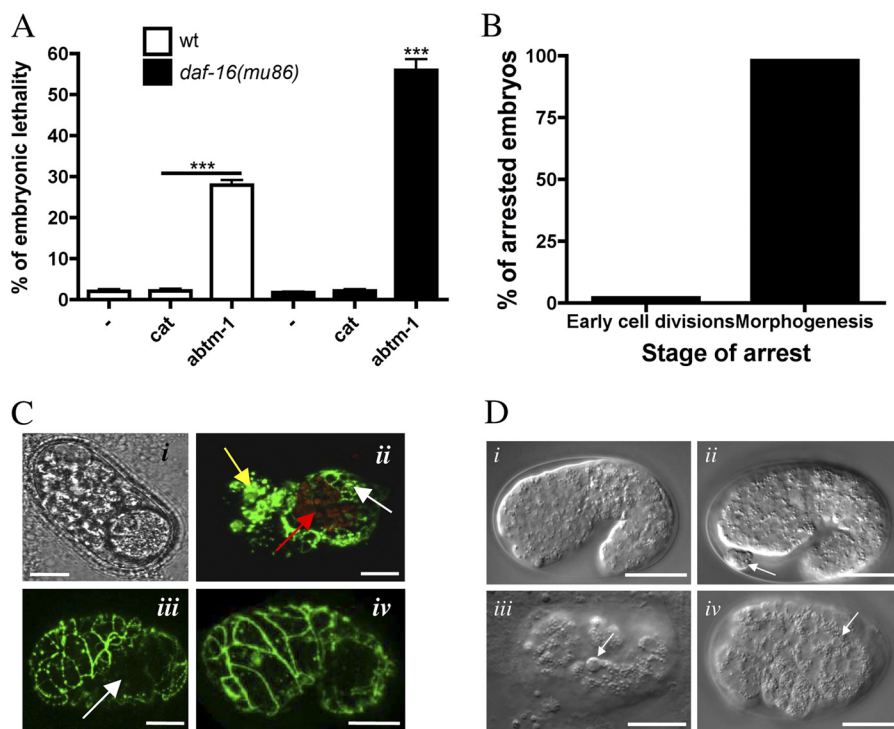
FIGURE 2. **Disruption of *abtm-1* produces embryonic lethality, which is further increased by depletion of *daf-16*.** *A*, embryonic lethality in the offspring of *abtm-1*(*RNAi*) worms in wild type and *daf-16*(*mu86*) backgrounds. *abtm-1*(*RNAi*) hermaphrodites produce 28% dead embryos, whereas depletion of *abtm-1* in *daf-16* mutants produce 56%. ***, Student's *t* test, *p* <0.0001. *B*, *abtm-1*(*RNAi*) produces arrest of embryos mostly during morphogenesis (96%). *C*, representative examples of *abtm-1*(*RNAi*)-arrested embryos. *C, panel i*, transmitted light image of an embryo arrested during the proliferation stage. *C, panel ii*, confocal image of an embryo arrested during morphogenesis, showing signs of cellular differentiation. The *yellow* and *white arrows* point to AJM-1::GFP expression, a cell-specific marker of epithelia, in the pharyngeal and epidermal cells, respectively. The *red arrow* indicates autofluorescent granules, characteristic of the intestinal cells. *C, panel iii*, confocal image of an embryo in which the epidermis has failed to migrate during ventral enclosure leaving the embryo incompletely enclosed as indicated by the *arrow*. *C, panel iv*, an embryo arrested during the last step of morphogenesis, elongation. The epidermis has enclosed most of the embryo, but it is highly disorganized. *D*, transmitted light images, from four-dimensional microscopic analysis. *D, panel i*, wild type embryo. *D, panel ii*, embryo arrested during morphogenesis showing the presence of internal tissues external to the embryo. *D, panels iii and iv*, embryos showing premature apoptotic events in the 9th generation. Apoptotic cells are indicated by *arrows*. All *scale bars* represent 10 μm.

ii). Therefore, ABTM-1 is required for appropriate embryonic morphogenesis in *C. elegans*.

abtm-1(RNAi) Embryos Have Premature, Putative Apoptotic Events—To investigate possible causes of the morphogenetic defects in *abtm-1*(*RNAi*) embryos, we used four-dimensional video microscopy and lineage analysis. The cell lineage of *C. elegans* is well defined so that every somatic cell can be traced (16, 57). Moreover, four-dimensional imaging is a well established tool for identifying and studying apoptosis (23, 24). In a wild type embryo the progeny of the "founder cell" AB (the anterior cell in the two-cell stage embryo) divide, in near synchrony, after each cell generation and can be readily tracked by four-dimensional video microscopy imaging. We recorded *abtm-1*(*RNAi*) and wild type embryos to identify differences in cell cycle length, fate specification, morphogenesis, and cell death. Six of the *abtm-1*(*RNAi*) embryos were analyzed in detail with respect to cell lineage and timing. We observed four phenotypic classes of *abtm-1*(*RNAi*) embryos (Table 1). *abtm-1*(*RNAi*) embryos have delayed cell divisions, cells that are excluded from the embryo and in extreme cases burst. In addition, two of the embryos showed a striking defect. Some cells in the 9th cell generation (ABalaaapp, ABprappap, and ABprppapa in one embryo, and most probably ABplpppapp in the other) underwent cell death, most probably by apoptosis (Fig. 2*D*). In normal embryos apoptosis occurs in specific cells in the

10th and the 11th cell generation, as a consequence of specific cell fate decisions. The presence of these putative premature apoptotic events may indicate that cells are activating the apoptotic pathway as consequence of cellular stress. *abtm-1*(*RNAi*) embryos also show increases in the cell cycle length (Table 1). The severity of this defect increases as development proceeds with late cells dividing much more slowly than the early blastomeres. On average the division of AB*xxxxxx*, the last cell division recorded, was nearly twice as long as the wild type division, and in extreme cases was nearly three times as long (Table 1). Again, this suggests that cellular metabolism is disrupted. In addition, in three embryos some cells were excluded from the body during morphogenesis (Fig. 2*D, panel ii*). Four-dimensional analysis, in one embryo, clearly identified 3 of 10 of these cells as neuronal cells of the ring ganglion (the specific cells are ABalapappap, ABalappaapa, and ABalapppaap).

abtm-1(RNAi) Animals Show Accumulation of Fe^{3+}—Our results above suggest that *abtm-1* animals have severe cellular defects. We sought to determine whether those *abtm-1*(*RNAi*) animals that reached adulthood have changes in their physiology reflecting the function of ABTM-1. Deletion of the yeast *ABCB7* homologue, *ATM1* (8), results in ferric iron (Fe^{3+}) overload. We therefore hypothesized that if *abtm-1* function is conserved in *C. elegans*, *abtm-1* knockdown should lead to a similar phenotype. To test this hypothesis, we sought to meas-

TABLE 1

Delayed cell divisions in *abtm-1(RNAi)* embryos

abtm-1(RNAi) embryos were analyzed by four-dimensional video microscopy and subsequent lineage analysis. Embryos were divided into four types based on the nature of the developmental defects observed. Delays during the development of all the embryos were measured, although we only show data of the four representative types. Numbers indicate the time (in minutes) to complete the cell cycle for the cell in the left column. Although some variability in the timing of cell cleavages occurs from embryo to embryo in the wild type (57), the difference compared with the reference published by Sulston in 1983 (57) is always smaller than 10% of the cell cycle length. We consider that a cell is dividing significantly slower than wild type when the length of its cell cycle is at least 20% longer than the wild type reference.

| Cycle cell	Wild type average mean time	Time for cell division (mins) (% of increment in cell cycle)[a]				*abtm-1(RNAi)* average mean time
		abtm-1(RNAi) type 1	*abtm-1(RNAi)* type 2	*abtm-1(RNAi)* type 3	*abtm-1(RNAi)* type 4	
	min					*min*
AB						
AB*x*	12.5		17 (36%)	19 (52%)	20 (60%)	16.4 (31%)
AB*xx*	14.6		20 (37%)	21 (44%)	24 (65%)	18.8 (29%)
AB*xxx*	16.4	27 (64%)	24 (45%)	24 (46%)	32 (94%)	23.0 (39%)
AB*xxxx*	23.9	41 (71%)	33 (37%)	36 (51%)	42 (76%)	33.0 (38%)
AB*xxxxx*	25.3	57 (125%)	45 (78%)	47 (86%)	63 (149%)	44.3 (75%)
AB*xxxxxx*	33.2	93 (179%)	55 (65%)	-	82 (146%)	61.0 (67%)
Phenotype[b]	(3)	Delayed development alone (2)	Delayed development and excluded cells (3)	Delayed development and explosion (1)	Delayed development and premature apoptosis (2)	

[a] The increment of the time in delayed cycles is shown in parentheses. To obtain the average of the increment, we included the cycles of all available embryos ($n = 8$).

[b] The lower row shows the phenotype for each type of *abtm-1(RNAi)* embryo. All types showed delayed development. Type 1 did not have any other apparent defects. Type 2 embryos had internal tissues on the exterior (Gex phenotype). Type 3 embryos burst, probably due to a defect in morphogenesis. Type 4 showed some premature apoptosis as well as morphogenetic defects. The number of embryos of each type that we observed is shown in parentheses.

ure iron levels in *abtm*-depleted animals. We also tested *frh-1(ok610)* worms that carry a loss of function allele in the frataxin (*frh-1*) gene (17) responsible for Friedreich ataxia (25). This molecule has been suggested to be involved in Fe-S cluster synthesis (reviewed by Stemmler *et al.* (26)), among other hypotheses (reviewed by Gonzalez-Cabo *et al.* (27)). Disruption of frataxin induces iron accumulation in many organisms, for example in yeast (28). Although total iron levels ($Fe^{2+} + Fe^{3+}$) in *abtm-1(RNAi)* animals did not show any significant difference to control animals, *abtm-1(tm2721)/+* mutants showed a sensible increase ($n \geq 3000$ for each strain tested) (Fig. 3*A*). In both cases Fe^{3+} was present at much increased levels in *abtm-1(RNAi)* (10-fold), *abtm-1(tm2721)/+* (16-fold), and also in *frh-1(ok610)/+* (18-fold) animals compared with wild type and *cat(RNAi)* controls (Fig. 3*B*).

Depletion of abtm-1 Causes Increased Oxidative Stress—As *abtm-1(RNAi)* animals show accumulation of Fe^{3+}, we sought to investigate if this caused increased oxidative stress. First, we tested the ability of *abtm-1(RNAi)* animals to cope with an externally induced increase in free radicals by measuring survival on exposure to paraquat (29, 30). Worm survival in the presence of a range of paraquat concentrations was measured. On 0 and 0.5 mM paraquat, the survival of *abtm-1(RNAi)* animals is unaltered (data not shown). However, at 5 and 10 mM paraquat, *abtm-1(RNAi)* worms show substantial reductions in survival (log-rank (Mantel-Cox) test $p < 0.0001$ for both paraquat concentrations) (Fig. 4*A*), suggesting that reductions in ABTM-1 cause increased sensitivity to oxidative stress.

We next examined whether *abtm-1(RNAi)* animals had increased levels of endogenous free radicals. We examined the expression of a *sod-3::GFP* reporter gene. SOD-3 is a mitochondrial manganese-dependent superoxide dismutase homologue and a known free radical scavenger. Expression of *sod-3::GFP* transgenes is known to be increased in response to increases in free radical production (31). *abtm-1* RNAi on animals carrying the *sod-3::GFP* transgene resulted in a greater than 2-fold increase in fluorescence compared with controls ($p < 0.001$; $n = 30$) (Fig. 4*B*).
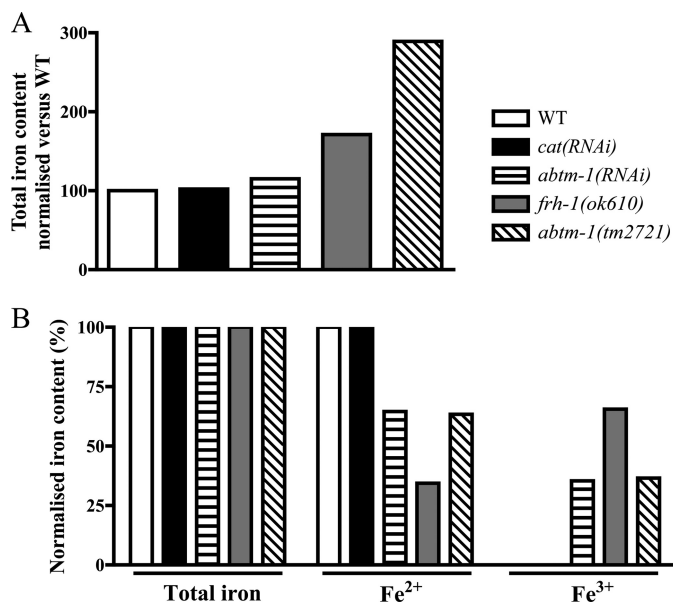
FIGURE 3. **Depletion of *abtm-1* induces accumulation of ferric iron.** *A, graph* shows total iron content, normalized to the wild type level in wild type, *cat(RNAi)*, *abtm-1(RNAi)*, *frh-1(ok610)* animals, and *abtm-1(tm2721)*. *B, graph* shows the percentage of ferrous and ferric iron in the same strains normalized to the total iron content in that strain. Fe^{3+} is increased in animals with reduced ABTM-1 or frataxin (FRH-1).

To confirm that ablation of *abtm-1* induces oxidative stress, we sought to investigate the effects of increased free radical levels *in vivo*. Thus, we measured protein carbonylation as amino acid carbonylation is caused by free radicals. To do this, we used an Oxyblot™ assay on *abtm-1(RNAi)*, wild type, and *cat(RNAi)* worms, together with frataxin mutant animals. *cat(RNAi)* and wild type worms show similar amounts of carbonylated proteins (Fig. 4*C, 1st* and *2nd lanes*), although the frataxin worms show an increase of 1.5-fold (Fig. 4*C, 4th lane*). Interestingly, the *abtm-1(RNAi)* worms show a 3.5-fold increase in carbonylated proteins (Fig. 4*C, 3rd lane*). Thus, the above evidence suggests that *abtm-1*-depleted animals are under significantly increased levels of oxidative stress, presumably resulting from increased Fe^{3+} levels.
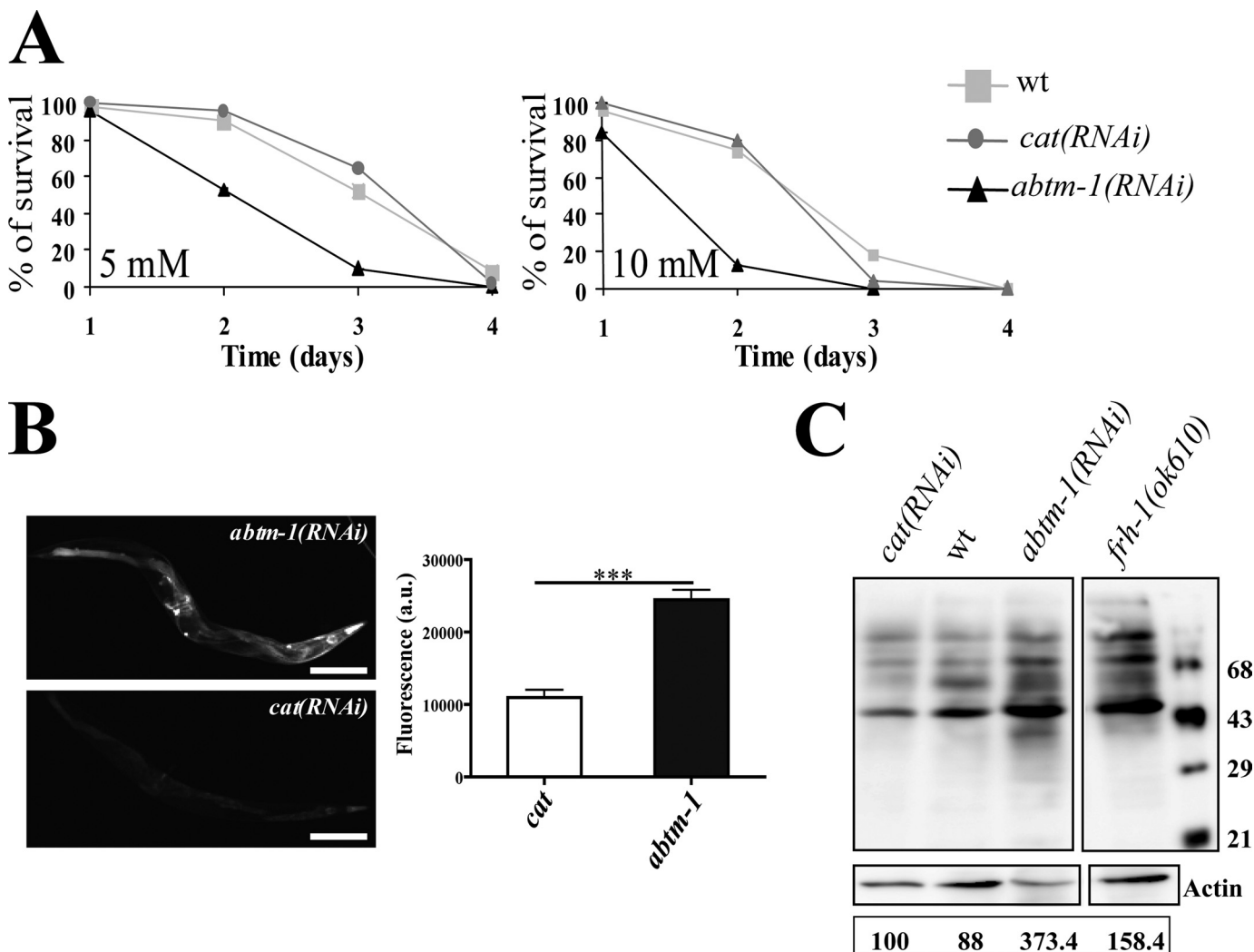
FIGURE 4. *abtm-1*(*RNAi*) worms are under oxidative stress. *A*, survival graphs of wild type, *abtm-1*(*RNAi*), and control animals *cat*(*RNAi*) grown in different concentrations of paraquat. At 5 and 10 mM, the survival of *abtm-1* depleted animals is significantly lower ($p < 0.0001$ in both cases) than control and wild type animals. *B*, transmission and fluorescent images of representative offspring from RNAi-treated worms containing the *sod-3::GFP* construct. *abtm-1*(*RNAi*) animals show an obvious increase in fluorescence (*i.e. sod-3* expression) compared with controls. *Scale bars* represent 50 μm. Quantification of this increase is shown below where the average fluorescence intensity (represented by arbitrary units), relative to the body area of each worm, in *sod-3::GFP* worms is plotted. *abtm-1*-depleted animals show a significant increase of expression compared with control worms ($p < 0.001$) ($n \geq 30$). *C*, Oxyblot™ assay on *cat*(*RNAi*), wild type *abtm-1*(*RNAi*), and *frh-1*(*ok610*) animals. Carbonylated proteins were quantified for each lane using MultiGauge software (FujiFilm). To allow for loading variation, values were normalized to the actin control. Final values are expressed as a percentage of the wild type value and are shown *below* each lane. It can be seen that *frh-1*(*ok610*) and the *abtm-1*(*RNAi*) worms show a marked increase in carbonylated proteins.

abtm-1(RNAi) Animals Have Increased Life Span, which Is Partially Dependent on daf-16/FOXO—Increased oxidative stress might be expected to reduce life span. However, the life span of *abtm-1* deficient worms is significantly increased compared with control animals (*abtm-1*(*RNAi*)) (median life span (ML) = 23 days *versus cat*(*RNAi*) ML = 19 days, $p < 0.0001$; supplemental Table S1) (Fig. 5*A*). Changes in the activity of the transcription factor *daf-16*/FOXO alter longevity in many organisms, including humans (32). Furthermore, *daf-16* is known to mediate both insulin and stress responses (20). Therefore, we tested for interactions between the effects on life span of *abtm-1* and *daf-16*. Interestingly, depletion of *abtm-1* in a *daf-16* loss of function background shows a partial increase in life span (Fig. 5*A*) (*daf-16*(*mu86*); *abtm-1*(*RNAi*) ML = 18 *daf-16*(*mu86*); *cat*(*RNAi*) ML = 17; supplemental Table S1), suggesting that the life span increase in *abtm-1*(*RNAi*) animals is partially dependent on DAF-16 function.

DAF-16 is known to relocate from the cytoplasm to the nucleus when activated (33). Therefore, we investigated the cellular localization of DAF-16 in *abtm-1* depleted worms by inducing *abtm-1* RNAi in animals that carry a functional DAF-16::GFP fusion (33). We observed that most *abtm-1*(*RNAi*) animals showed nuclear localization of DAF-16 in one or more tissues, suggesting that ablation of *abtm-1* induces signals that activate DAF-16.

abtm-1-depleted Adult Animals Have a Pleiotropic Phenotype, Including Defects in Locomotion and Rhythmic Behavior—Phenotypic analysis of adults (and embryos) is a prerequisite to our aim of establishing a model for XLSA/A that can be used for both mechanistic studies and screening for compounds that may be developed for clinical use. In *C. elegans*, mitochondrial mutants usually show a range of phenotypes, including developmental, physiological, and behavioral defects (reviewed by
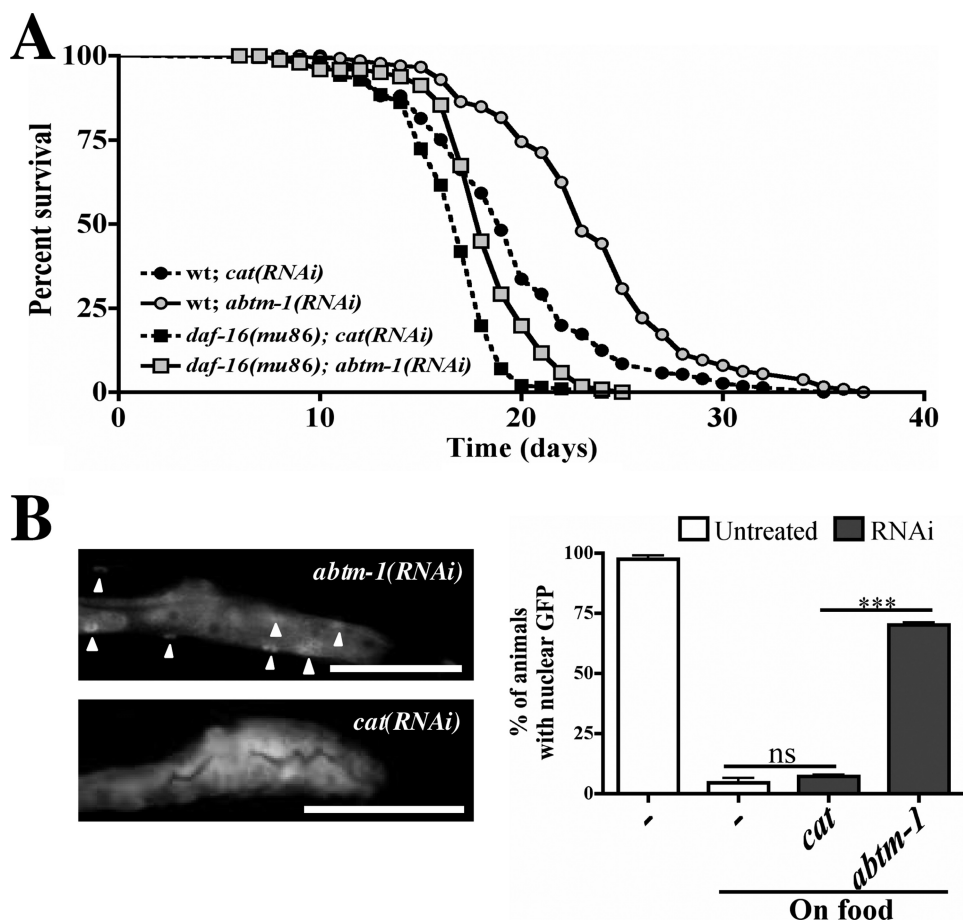
FIGURE 5. **Life span of *abtm-1*(*RNAi*) adults is increased in a partially *daf-16*–dependent manner.** *A*, life span curves of *abtm-1*(*RNAi*) worms in wild type and *daf-16*(*mu86*) mutant backgrounds. The life span of *abtm-1*-depleted animals is significantly longer than control worms ($p < 0.0001$). Induction of *abtm-1* RNAi also increases the life span of *daf-16*(*mu86*) mutants ($p < 0.0001$), but to a lesser extent (also see supplemental Table S1). *B*, *abtm-1* RNAi induces localization of DAF-16 in the nucleus in some tissues in 70% of worms. Starved animals (*first bar*) were used as positive control, as they show strong nuclear DAF-16 localization.

Tsang and Lemire (34)). This is indeed the case of *abtm-1*(*RNAi*) worms, which show a pleiotropic phenotype that includes developmental defects, growth, egg laying, ultradian rhythms (35), and locomotion defects (see above and supplemental material). Therefore *abtm-1*(*RNAi*) show similar traits to other mitochondrial mutants.

Disruption of Other Components of the Fe-S Cluster Biosynthesis Pathway Induces Similar Phenotypes to Depletion of abtm-1—In yeast, cytosolic Fe-S clusters are produced exclusively in the lumen of mitochondria. Fe-S clusters are produced using sulfur from cysteine in a reaction catalyzed by cysteine desulfurase (Nfs1p). Production also requires chaperones and scaffold proteins (Isa1p, Isa2p, Isu1p, and Isu2p) and redox proteins (Arh1p, Yah1p, and glutaredoxin-5), which supply Fe^{2+} (reviewed in Refs. 36, 37). Once produced, Fe-S clusters are either used in mitochondrial Fe-S-containing proteins or they are transported to the cytosol, by means of Atm1p/ABCB7, where they are used to produce cytosolic Fe-S-containing proteins (Fig. 6) (36). We investigated whether disrupting other steps in Fe-S synthesis would phenocopy the traits described above for *abtm-1*(*RNAi*) animals. We performed RNAi on the *C. elegans* orthologues of six Fe-S cluster biosynthesis genes (Wormbase release WS185) (Table 2 and Fig. 6). Knocking down these genes produces a range of phenotypes (*e.g.* disrupted defecation, extended life span, and larval arrest) all compatible with a mitochondrial phenotype (Table 2). Moreover, in all six cases, depletion produces significant embryonic arrest showing that disrupting the Fe-S cluster pathway compromises embryonic development in *C. elegans*. Both the mitochondrial phenotype and embryonic lethality recapitulate the phenotypes produced by ablation of *abtm-1*.

DISCUSSION

XLSA/A is an untreatable disease caused by mutations in the *ABCB7* gene. ABCB7 is believed to function in the mitochondrial transport of Fe-S clusters into the cytoplasm (8, 9). It is thought that defective Fe-S cluster transport leads to mitochondrial iron overload with subsequent free radical production and to reduced heme synthesis, which in turn results in reduced Fe-S-containing enzyme activity. These deficits may then lead to mitochondrial dysfunction and to the pathology of XLSA/A (11). Thus, XLSA/A is one of a growing number of mitochondrial diseases (38, 39). Using mutants and RNAi, we analyzed the effects of total and partial loss of function in *abtm-1,* the *C. elegans* homologue of *ABCB7*. Complete loss of *abtm-1* function is lethal, as is the loss of *ABCB7* in mice (6), and partial loss of function also leads to a substantial level of embryonic and larval arrest. Thus, as in other systems, *ABCB7*/

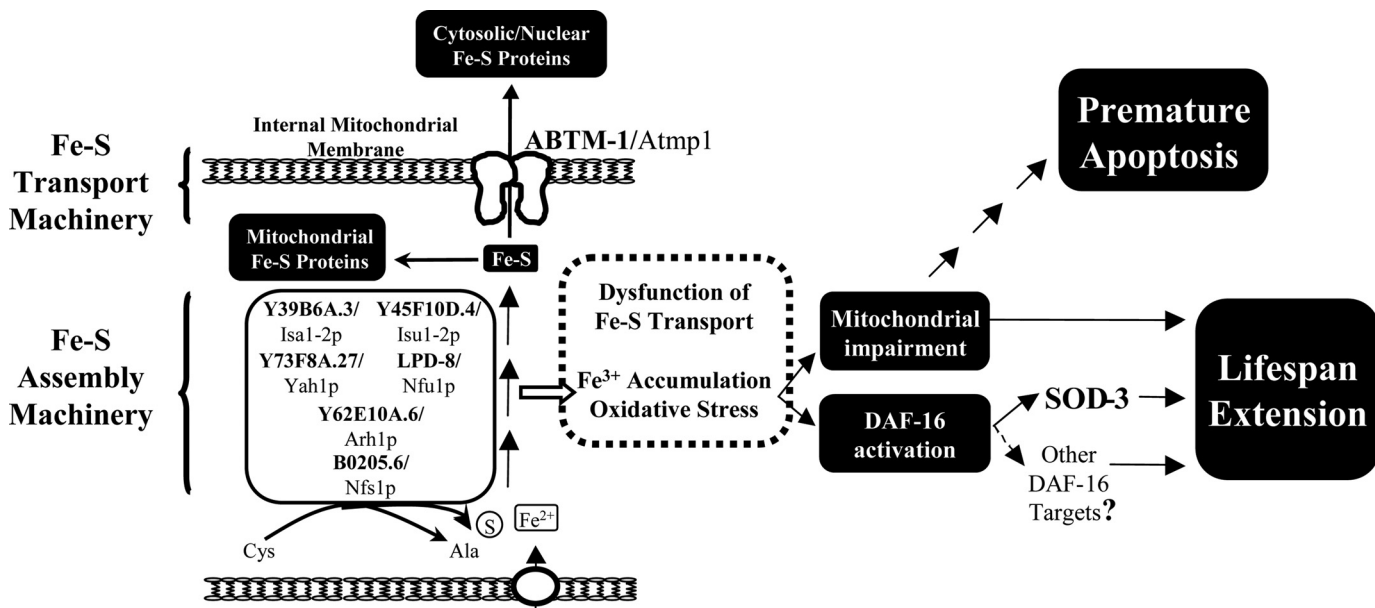## abtm-1 Depletion Induces Oxidative Stress and Cell Death

FIGURE 6. **Fe-S cluster synthesis pathway and our working model for the life span extension and apoptotic events caused by depletion of *abtm-1* in *C. elegans*.** The diagram shows the ABC transporter ABTM-1/Atm1p and some of the enzymes (ferredoxin reductase, Y62E10A.6/Arh1p; ferredoxin, Y73F8A.27/Yahp) and scaffolding proteins (LPD-8/Nfu1p, B0205.6/Nfs1p, Y39B6A.3/Isa1p, and Y45F10D.4/Isu1p) involved in the synthesis of Fe-S clusters. These molecules are represented by the name of the protein in *C. elegans* (*boldface*), and the corresponding *S. cerevisiae* homologue. Defects in Fe-S cluster synthesis caused by *abtm-1(RNAi)*, as indicated by the *box* surrounded by a *dotted line*, cause accumulation of iron, which in turn induces free radicals. The oxidative stress promoted by the free radicals is responsible for mitochondrial damage, which may lead to premature apoptosis and activation of DAF-16. Both the mitochondrial damage and DAF-16 activation may induce life span extension in individuals that survive embryogenesis. The life span extension induced by DAF-16 may be due to the expression of genes such as *sod-3*.

TABLE 2
Disruption of genes involved in Fe-S cluster synthesis produces a range of phenotypes

The coefficient of variation (CV) is reported as a percentage and is calculated from the average and S.D. as follows: $100 \times$ S.D./average.

Strain	Yeast putative homologue gene	% of Embryonic arrest (n)	Larval arrest	Defecation cycle (CV)	Life span
			%		
Wild type		2.1 (1597)	0	48 ± 3 (6 ± 1)	Normal
cat(RNAi)	NA[a]	1.9 (1641)	0	48 ± 1 (5 ± 1)	Normal
abtm-1(RNAi)	ATM1	27.9 (945)	<5	60 ± 3 (17 ± 3)	Long lived ($p < 0.001$)[b]
Y62E10A.6(RNAi)	ARH1	11.8 (543)	<5	77 ± 5 (14 ± 2)	Long lived ($p < 0.001$)[b]
lpd-8(RNAi)	NFU1	18.0 (389)	<5	50 ± 2 (8 ± 1)	Long-lived ($p < 0.001$)[b]
B0205.6(RNAi)	NFS1	39.5 (440)	100	NA	NA
Y73F8A.27(RNAi)	YAH1	48.8 (540)	100	NA	NA
Y39B6A.3(RNAi)	ISA1	63.1 (367)	100	NA	NA
Y45F10D.4(RNAi)	ISU1	84.1 (414)	100	NA	NA

[a] NA means not applicable.
[b] Log rank (Mantel-Cox) test was used.

abtm-1 is an essential gene. The use of RNAi enabled us to produce a model that recapitulates the partial loss of function found in XLSA/A patients. Partial loss of function results in arrested embryos and adults with increased Fe^{3+} levels, higher oxidative stress, increased life span, and a range of phenotypes characteristic of mutations that cause mitochondrial dysfunction. Expression analysis showed that ABTM-1 is a widely expressed mitochondrial protein that it is produced at particularly high levels in tissues that are expected to have high energy requirements, as is the case in humans and mice (3, 6). Thus our data show that, as in other models, *abtm-1* is an essential mitochondrial gene.

Depletion of *abtm-1* caused substantial embryonic arrest. Analysis of *abtm-1(RNAi)* embryos showed that arrest mostly occurs after the initial proliferative phase and usually during morphogenesis. Detailed analysis of early embryonic development, using four-dimensional imaging, showed that the embryos have slower cell divisions and that, strikingly, they exhibit putative premature apoptosis. These early defects may underlie later defects in morphogenesis. For example, the loss of cells due to putative apoptosis could result in the loss of cells or cell types that are required for morphogenesis. In particular the putative apoptotic cells observed in the *abtm-1(RNAi)* embryos belong to lineages that will give rise to neuroblasts, a cell type that is essential for proper epidermal migration during morphogenesis (21). In addition, disorganized cell division may result in the failure of important inductive developmental signaling events in the early embryo, again leading to the loss of particular cells and cell types. The early defects in these embryos could all result from an abnormal mitochondrial function. For example, apoptosis may result from defective mitochondrial function (40). Similarly the cell cycle has a high energy demand (41) and may be retarded due to reduced ATP levels caused by poor mitochondrial func-

tion. Interestingly, a delay in cell cycle progression has been described in *Drosophila* as a result of a mutation in *tenured*, a gene encoding mitochondrial cytochrome oxidase subunit Va (42). Thus defects in *abtm-1* may cause lethality in embryos due to a pyramid of effects, which emanate from mitochondrial dysfunction.

Although depletion of *abtm-1* by RNAi produced substantial lethality, a significant proportion of worms were able to survive to adulthood. This presumably reflects different degrees of *abtm-1* depletion in different animals. Animals that survived to adulthood demonstrated a range of phenotypes, including disrupted defecation, egg laying, and locomotion suggesting a widespread perturbation of physiological function in several tissues, including neurons. This range of phenotypes is reminiscent of the pleiotropy observed in other mitochondrial mutants, such as *frh-1*, the *C. elegans* homologue of frataxin (17, 43). Interestingly, the role of frataxin, although still controversial (see Refs. 27, 44, 45), has also been linked to Fe-S cluster production (for a review see Rouault and Tong (46)). Therefore, phenotypes caused by depletion of both molecules may be due to similar cellular stresses. We propose that this pleiotropic phenotype results from defects in Fe-S cluster metabolism. In support of this, depleting other genes involved in Fe-S biogenesis and transport results in phenotypes that share some of the features of *abtm-1*(*RNAi*) worms. It is interesting to note that RNAi on four of these genes (B0205.6/*NFS1*, Y73F8A.27/*YAH1*, Y39B6A.3/*ISA1*, and Y45F10D.4/*ISU1*) produced 100% embryonic and larval arrest in the offspring. This may reflect a more severe mitochondrial defect in these worms, perhaps because they affect key steps in the synthesis of all Fe-S clusters in contrast to *abtm-1*, which only mediates transport of cytosolic Fe-S clusters. Differences in the strength of the RNAi may also explain differences in the severity of phenotypes.

We observed a substantial increase in Fe^{3+} in *abtm-1* animals. *abtm-1* mutant animals also showed an increase in total iron content. Disruption of iron homeostasis underlies many human disorders. This is probably also the case in XLSA/A where it has been suggested that the pathological condition may be a consequence of mitochondrial iron accumulation. In this regard, the yeast mutant *atm1Δ* shows accumulation of ferric phosphate (47). It is suggested that ferrous iron (Fe^{2+}) enters mitochondria where it is oxidized to Fe^{3+}. Excess ferric iron, due to inactivity of ABTM-1, has been shown in Atm1/ABCB7-depleted yeast (28, 47, 48). Thus our results are compatible with previous studies.

abtm-1 animals have increased oxidative stress as measured by a number of approaches. One implication of the increase in oxidative stress might be expected to be a decrease in life span; however, these worms actually have increased life span. This paradox may be explained by hormesis. In hormesis, a beneficial biological response in a cell or organism is initiated by a nonlethal detrimental stress. The response is primarily aimed at counteracting the damage produced by that stress, but it also results in an increased life expectancy. This phenomenon has been documented in yeast (49) and *C. elegans* (50, 51) and indeed many mitochondrial mutants in *C. elegans* that do not compromise survival also show life span extension (10, 52). Thus, in *abtm-1*(*RNAi*) animals, the activation of scavenging

molecules that promote cell survival, in response to the production of free radicals in mitochondria, may in turn increase life span. This may be reflected in the nuclear localization of DAF-16 and the increased expression of *sod-3*, both of which are markers of increased oxidative stress but are also, presumably, protective.

daf-16 is a master regulator of life and health span (53), and it is widely implicated in stress and related responses. DAF-16 appears to play an important role in the effects of *abtm-1* depletion suggesting that increased stress is a key determinant of the effects of *abtm-1* ablation, probably in response to free radical production. Increased nuclear localization of DAF-16 in *abtm-1*(*RNAi*) worms strongly suggests that it is being activated. DAF-16 may in turn induce the expression of *sod-3*, among other protective genes. The embryonic arrest caused by depletion of *abtm-1* is enhanced in a *daf-16* null background, suggesting that the presence of *daf-16* is able to protect against *abtm-1*(*RNAi*)-mediated damage caused by Fe^{3+} accumulation and free radical production. In addition, the increase in life span observed in *abtm-1* ablated animals is, at least, partially dependent on DAF-16. This may be explained if the putative hormesis discussed above is *daf-16*-dependent. Indeed, DAF-16 may act as a mediator of hormesis in *C. elegans*, upon activation by cellular stress (54). The increase in life span cannot be completely attributed to the action of DAF-16 and its downstream targets, as *daf-16*(*mu86*);*abtm-1*(*RNAi*) animals still have an increase in life span, suggesting that other forms of life span extension such as mitochondrial malfunction (Fig. 5*C*) or calorific restriction could be involved.

Model systems are critical to our ability to understand these processes. We have established a *C. elegans* model of the human disease XLSA/A. The ability to use a genetically tractable metazoan in the study of XLSA/A, and other mitochondrial diseases, should improve our understanding of the mechanisms that underlie these conditions. *C. elegans* enables the use of high throughput automated RNAi screens, using for example embryonic lethality, to identify genetic interactions (55). *C. elegans* can also be used in high throughput compound screens (56) or in the testing of drug candidates such as free radical scavenging molecules or activators of cell survival pathways that diminish cellular stress.

REFERENCES

1. Pagon, R. A., Bird, T. D., Detter, J. C., and Pierce, I. (1985) *J. Med. Genet.* **22,** 267–273
2. Allikmets, R., Raskind, W. H., Hutchinson, A., Schueck, N. D., Dean, M., and Koeller, D. M. (1999) *Hum. Mol. Genet.* **8,** 743–749
3. Savary, S., Allikmets, R., Denizot, F., Luciani, M. F., Mattei, M. G., Dean, M., and Chimini, G. (1997) *Genomics* **41,** 275–278
4. Maguire, A., Hellier, K., Hammans, S., and May, A. (2001) *Br. J. Haematol.* **115,** 910–917
5. Bekri, S., Kispal, G., Lange, H., Fitzsimons, E., Tolmie, J., Lill, R., and Bishop, D. F. (2000) *Blood* **96,** 3256–3264
6. Pondarré, C., Antiochos, B. B., Campagna, D. R., Clarke, S. L., Greer, E. L., Deck, K. M., McDonald, A., Han, A. P., Medlock, A., Kutok, J. L., Ander-

son, S. A., Eisenstein, R. S., and Fleming, M. D. (2006) *Hum. Mol. Genet.* **15,** 953–964

7. Pondarre, C., Campagna, D. R., Antiochos, B., Sikorski, L., Mulhern, H., and Fleming, M. D. (2007) *Blood* **109,** 3567–3569

8. Kispal, G., Csere, P., Guiard, B., and Lill, R. (1997) *FEBS Lett.* **418,** 346–350

9. Kispal, G., Csere, P., Prohl, C., and Lill, R. (1999) *EMBO J.* **18,** 3981–3989

10. Cavadini, P., Biasiotto, G., Poli, M., Levi, S., Verardi, R., Zanella, I., Derosas, M., Ingrassia, R., Corrado, M., and Arosio, P. (2007) *Blood* **109,** 3552–3559

11. Wingert, R. A., Galloway, J. L., Barut, B., Foott, H., Fraenkel, P., Axe, J. L., Weber, G. J., Dooley, K., Davidson, A. J., Schmid, B., Schmidt, B., Paw, B. H., Shaw, G. C., Kingsley, P., Palis, J., Schubert, H., Chen, O., Kaplan, J., and Zon, L. I. (2005) *Nature* **436,** 1035–1039

12. Lewis, J. A., and Fleming, J. T. (1995) *Methods Cell Biol.* **48,** 3–29

13. Mello, C., and Fire, A. (1995) *Methods Cell Biol.* **48,** 451–482

14. Miguel-Aliaga, I., Culetto, E., Walker, D. S., Baylis, H. A., Sattelle, D. B., and Davies, K. E. (1999) *Hum. Mol. Genet.* **8,** 2133–2143

15. Zwaal, R. R., Ahringer, J., van Luenen, H. G., Rushforth, A., Anderson, P., and Plasterk, R. H. (1996) *Cell* **86,** 619–629

16. Schnabel, R., Hutter, H., Moerman, D., and Schnabel, H. (1997) *Dev. Biol.* **184,** 234–265

17. Vázquez-Manrique, R. P., González-Cabo, P., Ros, S., Aziz, H., Baylis, H. A., and Palau, F. (2006) *FASEB J.* **20,** 172–174

18. Claros, M. G., and Vincens, P. (1996) *Eur. J. Biochem.* **241,** 779–786

19. Rose, A. M., Baillie, D. L., and Curran, J. (1984) *Mol. Gen. Genet.* **195,** 52–56

20. Baumeister, R., Schaffitzel, E., and Hertweck, M. (2006) *J. Endocrinol.* **190,** 191–202

21. Chisholm, A. D., and Hardin, J. (2005) in *WormBook* (Priess, J. R., and Seydoux, G., eds) pp. 1–22, doi:10.1895/wormbook.1.35.1

22. Köppen, M., Simske, J. S., Sims, P. A., Firestein, B. L., Hall, D. H., Radice, A. D., Rongo, C., and Hardin, J. D. (2001) *Nat. Cell Biol.* **3,** 983–991

23. Ellis, H. M., and Horvitz, H. R. (1986) *Cell* **44,** 817–829

24. Kinchen, J. M., Cabello, J., Klingele, D., Wong, K., Feichtinger, R., Schnabel, H., Schnabel, R., and Hengartner, M. O. (2005) *Nature* **434,** 93–99

25. Campuzano, V., Montermini, L., Moltò, M. D., Pianese, L., Cossée, M., Cavalcanti, F., Monros, E., Rodius, F., Duclos, F., Monticelli, A., Zara, F., Cañizares, J., Koutnikova, H., Bidichandani, S. I., Gellera, C., Brice, A., Trouillas, P., De Michele, G., Filla, A., De Frutos, R., Palau, F., Patel, P. I., Di Donato, S., Mandel, J. L., Cocozza, S., Koenig, M., and Pandolfo, M. (1996) *Science* **271,** 1423–1427

26. Stemmler, T. L., Lesuisse, E., Pain, D., and Dancis, A. (2010) *J. Biol. Chem.* **285,** 26737–26743

27. González-Cabo, P., Llorens, J. V., Palau, F., and Moltó, M. D. (2009) *Adv. Exp. Med. Biol.* **652,** 247–261

28. Lesuisse, E., Santos, R., Matzanke, B. F., Knight, S. A., Camadro, J. M., and Dancis, A. (2003) *Hum. Mol. Genet.* **12,** 879–889

29. Ishii, N., Takahashi, K., Tomita, S., Keino, T., Honda, S., Yoshino, K., and Suzuki, K. (1990) *Mutat. Res.* **237,** 165–171

30. Yamamoto, K., Honda, S., and Ishii, N. (1996) *Mutat. Res.* **358,** 1–6

31. Essers, M. A., de Vries-Smits, L. M., Barker, N., Polderman, P. E., Burgering, B. M., and Korswagen, H. C. (2005) *Science* **308,** 1181–1184

32. Willcox, B. J., Donlon, T. A., He, Q., Chen, R., Grove, J. S., Yano, K., Masaki, K. H., Willcox, D. C., Rodriguez, B., and Curb, J. D. (2008) *Proc. Natl. Acad. Sci. U.S.A.* **105,** 13987–13992

33. Henderson, S. T., and Johnson, T. E. (2001) *Curr. Biol.* **11,** 1975–1980

34. Tsang, W. Y., and Lemire, B. D. (2003) *Biochim. Biophys. Acta* **1638,** 91–105

35. Baylis, H. A. (2005) *Cell* **123,** 5–7

36. Lill, R., and Mühlenhoff, U. (2006) *Annu. Rev. Cell Dev. Biol.* **22,** 457–486

37. Rouault, T. A., and Tong, W. H. (2005) *Nat. Rev. Mol. Cell Biol.* **6,** 345–351

38. Zeviani, M., and Carelli, V. (2003) *Curr. Opin. Neurol.* **16,** 585–594

39. Zeviani, M., and Carelli, V. (2007) *Curr. Opin. Neurol.* **20,** 564–571

40. Liu, X., Kim, C. N., Yang, J., Jemmerson, R., and Wang, X. (1996) *Cell* **86,** 147–157

41. Murray, A., and Hunt, T. (1993) *The Cell Cycle*, pp. 42–65, Oxford University Press, Oxford

42. Mandal, S., Guptan, P., Owusu-Ansah, E., and Banerjee, U. (2005) *Dev. Cell* **9,** 843–854

43. Ventura, N., Rea, S., Henderson, S. T., Condo, I., Johnson, T. E., and Testi, R. (2005) *Aging Cell* **4,** 109–112

44. Palau, F. (2001) *Int. J. Mol. Med.* **7,** 581–589

45. Wilson, R. B. (2006) *Semin. Pediatr. Neurol.* **13,** 166–175

46. Rouault, T. A., and Tong, W. H. (2008) *Trends Genet.* **24,** 398–407

47. Miao, R., Kim, H., Koppolu, U. M., Ellis, E. A., Scott, R. A., and Lindahl, P. A. (2009) *Biochemistry* **48,** 9556–9568

48. Miao, R., Martinho, M., Morales, J. G., Kim, H., Ellis, E. A., Lill, R., Hendrich, M. P., Münck, E., and Lindahl, P. A. (2008) *Biochemistry* **47,** 9888–9899

49. Kharade, S. V., Mittal, N., Das, S. P., Sinha, P., and Roy, N. (2005) *FEBS Lett.* **579,** 6809–6813

50. Cypser, J. R., and Johnson, T. E. (2002) *J. Gerontol. A Biol. Sci. Med. Sci.* **57,** B109–114

51. Schulz, T. J., Zarse, K., Voigt, A., Urban, N., Birringer, M., and Ristow, M. (2007) *Cell Metab.* **6,** 280–293

52. Feng, J., Bussière, F., and Hekimi, S. (2001) *Dev. Cell* **1,** 633–644

53. Hsu, A. L., Murphy, C. T., and Kenyon, C. (2003) *Science* **300,** 1142–1145

54. Kenyon, C. (2005) *Cell* **120,** 449–460

55. Lehner, B., Crombie, C., Tischler, J., Fortunato, A., and Fraser, A. G. (2006) *Nat. Genet.* **38,** 896–903

56. Ségalat, L. (2006) *ACS Chem. Biol.* **1,** 277–278

57. Sulston, J. E., Schierenberg, E., White, J. G., and Thomson, J. N. (1983) *Dev. Biol.* **100,** 64–119